Available online at www.sciencedirect.com
ScienceDirect
Journal of the European Ceramic Society 29 (2009) 3023–3029
www.elsevier.com/locate/jeurceramsoc

Distribution of Σ3 misorientations in polycrystalline strontium titanate

Shao-Ju Shih, Catherine Bishop [a], David J.H. Cockayne *

Department of Materials, University of Oxford, Parks Road, Oxford OX1 3PH, United Kingdom

Received 12 March 2009; accepted 16 April 2009
Available online 17 May 2009

Abstract

$SrTiO_3$ is a potential electrolyte material for solid-oxide fuel cells due to its high ion conductivity. Grain boundaries (GBs) play an important role in bulk ion conductivity. It has been reported that the resistance of Σ3 GBs is much lower than the general GB in $SrTiO_3$. In order to clarify the conflicting reports on the prevalence of Σ3 GBs in $SrTiO_3$, grain size and GB misorientations in Nb-doped and undoped $SrTiO_3$ have been investigated as a function of annealing time. The observations suggest that the prevalence of both low-angle GBs and Σ3 GBs is strongly correlated to both abnormal grain growth and annealing time. In particular, the Σ3 GB population approaches that predicted by the Mackenzie random distribution when abnormal grain growth dominates.

Keywords: Abnormal grain growth; Grain boundaries; Perovskites; Fuel cells; EBSD

1. Introduction

Strontium titanate ($SrTiO_3$) is an important perovskite-structured material, having superior electronic properties for various applications, including for solid-oxide fuel cells (SOFC)[1,2] and grain boundary barrier layer capacitors.[3,4] For SOFC, due to its high ion conductivity and good thermal stability at intermediate temperatures (600–800 °C), $SrTiO_3$ has been identified as a potential electrolyte material.[1,2] In the SOFC electrolytes, the ion conductivity of $SrTiO_3$ is attributed to vacancy migration,[1,2] which relates to GB properties. The main reason is that the GBs impede the transport of charge, and the resistance of the interface is attributed to the existence of a surface electrical potential.[5] The electrical potential barrier is related to the individual defect formation energies, dopant concentration, temperature, oxygen pressure, and the dominant charge compensation mechanism in the bulk.[6] Since the individual formation energies of defects such as cation and anion vacancies can differ, there should be an excess of the species with lower formation energy at a grain boundary at equilibrium. The GB becomes non-stoichiometric with a net charge. That net charge is compensated with space charge regions near the grain boundary that maintain global electro-neutrality. The GB can be modelled as a double Schottky barrier and its excess resistance related to the charge carrier concentrations next to the GB core and in the bulk. The local equilibrium of defects with a GB depends on the character of the GB and can vary from GB to GB in a microstructure.

Since special properties (e.g. low GB energy) of coincidence-site lattice (CSL) GBs were proposed in polycrystalline materials,[7,8] CSL GBs have been used to correlate with the electronic properties in perovskites. For example, in barium titanate ($BaTiO_3$), Σ3 GBs having no positive temperature effect are reported to be PTC inert.[9,10] In $SrTiO_3$, to understand how the Σ3 GBs contribute to the electronic properties, the atomic structure and energy of Σ3 GBs have been examined by various research groups. Initially, using high resolution transmission electron microscopy, Kienzle et al.[11] and Ernst et al.[12] characterized the atomic structure in bicrystals and polycrystals of $SrTiO_3$, respectively. Later, using density functional calculations, Hutt et al.[13] calculated the electronic structure of the Σ3 GBs based on Kienzle's[11] observations, and concluded that there is no evidence to support the existence of space charge layers at Σ3 GBs. This result suggests that the resistance of Σ3 GBs is much lower than the general GBs because no space charge layer impedes ion migration. So, an increased population of Σ3 GBs results in a higher ion conductivity in $SrTiO_3$.

* Corresponding author. Tel.: +44 186 527 3654; fax: +44 186 528 3329.
E-mail address: david.cockayne@materials.ox.ac.uk (D.J.H. Cockayne).
[a] Current address: Mechanical Engineering Department, University of Canterbury, Private Bag 4800, Christchurch, 8140, New Zealand.

0955-2219/$ – see front matter © 2009 Elsevier Ltd. All rights reserved.
doi:10.1016/j.jeurceramsoc.2009.04.020

The bulk ion conductivity is expected to depend on the number distribution of Σ3 GBs. However, there are conflicting reports about the distribution of Σ3 misorientations in $SrTiO_3$. Ernst et al.[14] reported that in titanate-based ceramics ($SrTiO_3$, $BaTiO_3$ and $Pb(Zr_xTi_{1-x})O_3$) GBs with Σ3 misorientations are found significantly more frequently than expected from a random misorientation distribution. However, Saylor et al.[15] reported that the GBs with Σ3 misorientations occur with a random distribution in undoped $SrTiO_3$ and they suggested that the result of Ernst et al.[14] may be due to Fe-doping and TiO_2 excess. Seaton and Leach investigated the relationship between the microstructure and the populations of low Σ GBs for donor-doped (Pb, Sr, and Ca) $BaTiO_3$ during the early stages of sintering (less than 1 h).[16,17] They found that the proportion of low Σ GBs increased during the first 30 min and then became stable. Recently Park et al.[18] investigated the low Σ misorientations in undoped $SrTiO_3$ as a function of annealing time (1 and 16 h) and came to a different conclusion. They found that the proportion of Σ3 misorientations decreased with annealing time.

In order to clarify whether preferred Σ3 misorientations develop in $SrTiO_3$, this study investigates (i) grain size distributions, (ii) grain misorientation distributions and (iii) Σ3 GB distributions in undoped and Nb-doped $SrTiO_3$ in samples annealed for different times. These three distributions have been determined by electron backscatter diffraction (EBSD).

2. Experimental

2.1. Ceramic synthesis

Samples were provided within the INCEMS Project by Prof. Hoffmann and Dr Bäurer (University of Karlsruhe). For a control experiment, undoped $SrTiO_3$ samples were prepared from $SrCO_3$ (99.9+ wt%, Sigma–Aldrich, Milwaukee, United States) and TiO_2 (99.9+ wt% Sigma–Aldrich, Milwaukee, United States) powders by the mixed-oxide route. The mixture of $0.996SrCO_3$ to $1TiO_2$ (molar ratio) was ball-milled for 4 h with 2-propanol in an attrition mill using ZrO_2 balls, calcinated at 975 °C in air for 6 h and then ball-milled for 16 h in a planetary mill. The calcined powder was uniaxially pressed into discs, isostatically densified at 400 MPa, sintered at 1425 °C in oxygen for 20 h and then quenched to room temperature. Nb-doped $SrTiO_3$ powder was prepared from Nb_2O_5 (99.9 wt%, ChemPur, Karlsruhe, Germany) and the same $SrCO_3$ and TiO_2 powders. The powder mixture of $0.994SrCO_3$, $0.006Nb_2O_5$ and $0.988TiO_2$ (molar ratio) was processed by the same ball-milling and calcination procedures, and annealed at 1425 °C in oxygen for 1, 2, 4 or 20 h, and then quenched to room temperature. Dilatometry showed that samples attained greater than 97% of the theoretical density after short times at temperature.[19]

2.2. Grain size and misorientation

Grain size and grain misorientation analyses were carried out using EBSD. In order to obtain precise misorientation data, it is important to collect good quality Kikuchi maps from EBSD, and this requires a well polished and uncontaminated sample surface.[20] The EBSD samples were prepared by mechanical grinding with SiC abrasive papers (800, 1200, 2000 mesh) and then polishing with a succession of 9, 3, 1 and 0.1 μm diamond cloths. The samples were chemically etched in a $95H_2O$–4HCl–1HF (by volume percent) solution for 30 s to remove surface contamination caused by sample polishing.

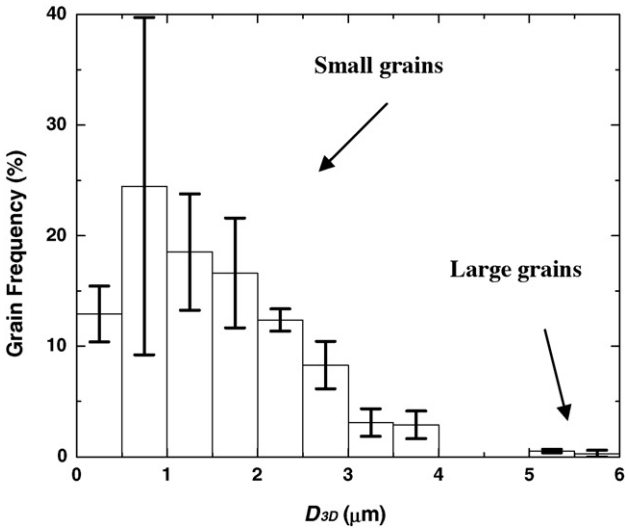

Fig. 1. The 3-D grain size ($D_{3\text{-D}}$) distribution in Nb-doped $SrTiO_3$ sintered for 1 h at 1425 °C in oxygen. Error bars indicate the standard deviation of grain size measurement from different sets measured on three regions that contain at least 600 grains each.

EBSD Kikuchi patterns were obtained using a JSM 6300F SEM, with an 80 μA beam current and 0.19–4.64 μm step size at a working distance of 15 mm. The step size was at least ten times smaller than the average grain size (diameter), to give precise measurements. The sample was inclined at 70° to the 20 kV incident electron beam. Analysis of the Kikuchi patterns was carried out with computer software (Inca, Oxford Instruments, UK). For grain determination, two neighbouring pixels were considered to be in the same grain if they had a misorientation angle less than 3°, and GBs were identified between adjacent grains.[18] The grain boundary distribution statistics were based on the number of grain boundary segments identified between misorientated pixels.

In EBSD, the most common way to obtain the two-dimensional (2-D) grain size distribution is by using the equivalent circle diameter.[21,22] However, a description of grains (i.e. grain size) in three-dimensions (3-D) gives more physical insight than that in 2-D. In this study the 3-D grain size distribution was extracted from the equivalent circle diameters using the method developed by Underwood.[23] Error bars indicate the standard deviation of grain size measurement from different sets measured on three regions that each contain at least 600 grains. Bi-modal distributions of 3-D grain size are obtained, as shown in Fig. 1. This bi-modal distribution associates with abnormal grain growth, which is frequently found in $SrTiO_3$.[24,25] The overall grain size (G) of a sample was calculated from $G = \bar{D}_{3\text{-D},l} \times N_l/(N_l + N_s) + \bar{D}_{3\text{-D},s} \times N_s/(N_l + N_s)$, where $\bar{D}_{3\text{-D},l}$ and $\bar{D}_{3\text{-D},s}$ are the average values of 3-D grain size of large

and small grain populations, respectively, and N_l and N_s are the number of large grains and the small grains, respectively.

3. Results and discussion

3.1. Microstructure and grain size distribution

Fig. 2(a)–(d) shows the typical EBSD grain orientation image maps (OIMs) along the sample normal direction with respect to the stereographic triangle for 1, 2, 4 and 20 h annealing, respectively, for the Nb-doped sample, and Fig. 2(e) for 20 h annealing for the undoped sample. In this study, all samples had a Ti-excess (Sr/Ti = 0.996 for undoped and 0.994 for Nb-doped), which should cause abnormal grain growth.[26]

As shown in Fig. 2(a)–(e), there are two groups of grains, large and small. The 2-D grain size distributions were extracted from the OIMs and converted to 3-D distributions for all samples. For example, Fig. 1 shows the 3-D histogram from Fig. 2(a) (1 h annealing) and the typical bi-modal distribution. Using the 3-D histogram, quantitative information about the bi-modal distribution can be obtained. For example, at 1 h annealing, the overall grain size G is 1.5 μm, including a small outlying number (0.8%) of larger grains of size 5.4 μm.

Fig. 3 shows the bi-modal grain sizes of Nb-doped $SrTiO_3$ samples as a function of annealing time. In most cases (1, 2, and 4 h), there is a clear separation between those grains that are small and large in size. These results (bi-modal distribution) are evidence of abnormal grain growth, with grains in the larger size group in 1, 2 and 4 h annealed samples being identified as those that have undergone abnormal grain growth. With increasing annealing time, the fraction of large grains increases as does their overall grain size. By 20 h, all small grains were consumed by

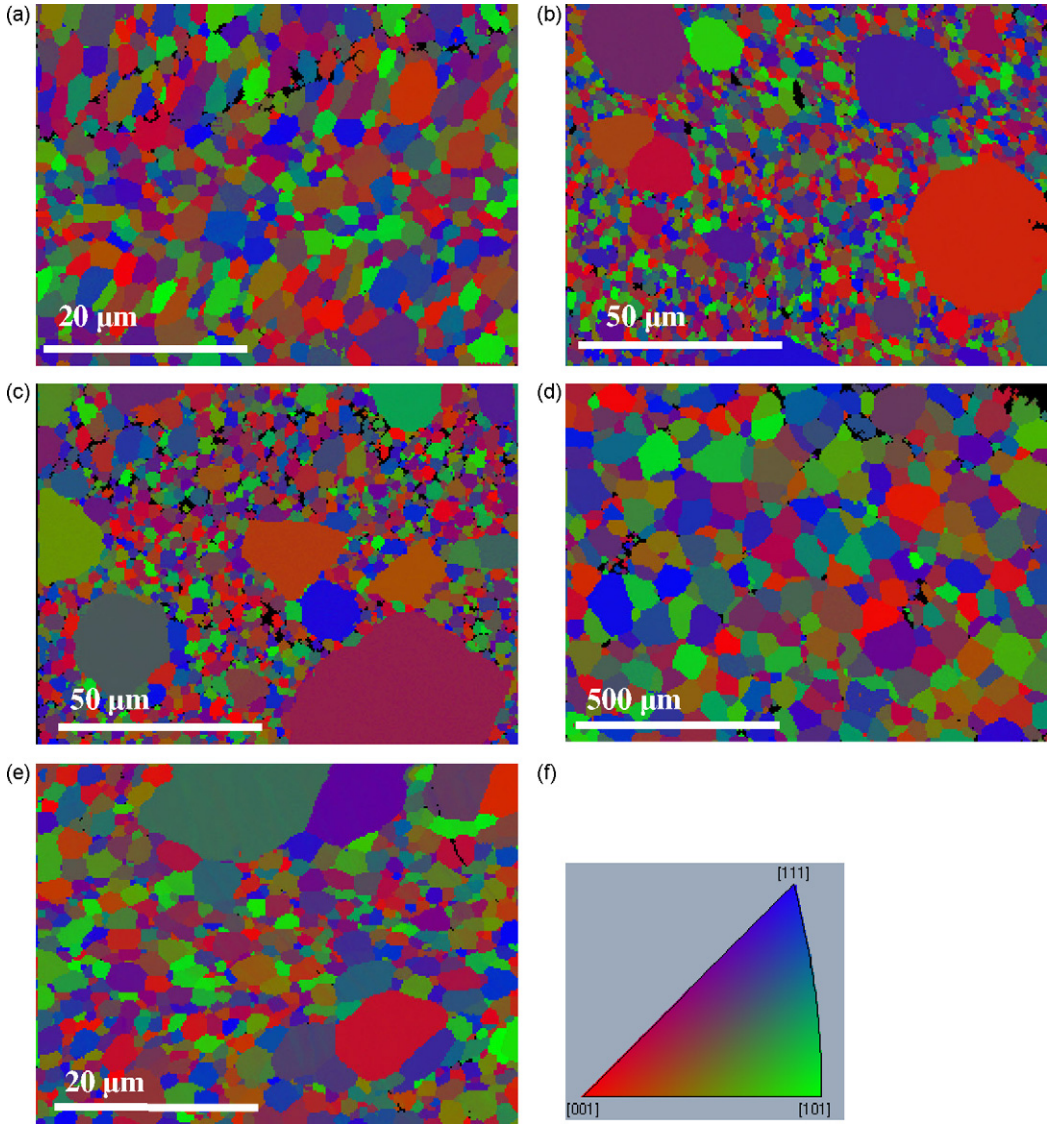

Fig. 2. Typical OIMs showing the orientation and shape of the grains obtained in Nb-doped $SrTiO_3$ samples annealed for (a) 1 h, (b) 2 h (c) 4 h and (d) 20 h and (e) the undoped $SrTiO_3$ sample annealed for 20 h. Samples were annealed at 1425 °C in oxygen. Colour-map in OIMs corresponds to the stereographic triangle of (f) and represents the crystal orientation normal to the specimen surface.

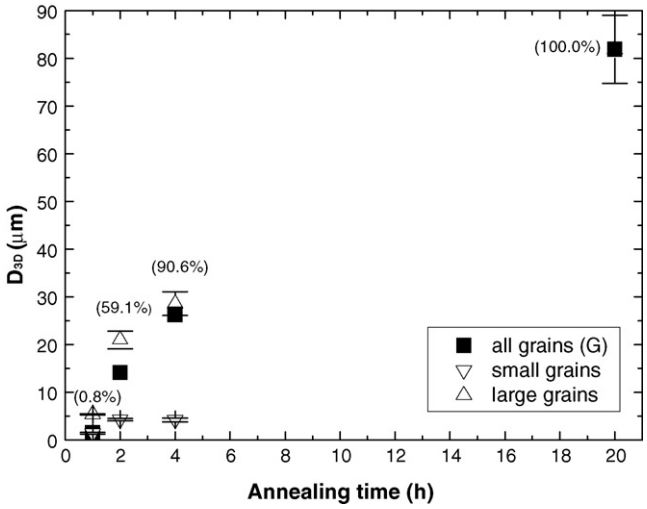

Fig. 3. 3-D grain size of Nb-doped $SrTiO_3$ samples as a function of annealing time. Samples sintered at 1425 °C in oxygen. The percentage of large grains is given in brackets. Error bars indicate the standard deviation of grain size measurement from different sets measured on three regions that contain at least 600 grains each.

the large grains. It should be noted that although the 20 h sample has a unimodal grain size distribution that would be identified with normal grain growth, from the grain growth evolution it is clear that these grains are from the large grains in the 1, 2, and 4 h annealed samples. So, these grains at 20 h are recognized as large grains in this study.

A comparison between the undoped (Fig. 2(d)) and doped (Fig. 2(e)) samples, sintered under the same conditions and for the same time of 20 h, shows that abnormal grain growth is much faster in the Nb-doped samples than in the undoped samples. The doped sample has an overall grain size $G = 81.9\ \mu m$ from 100% large grains compared to $G = 4.0\ \mu m$ with 16.7% large grains in the undoped sample. This result is in agreement with earlier studies which show that different grain growth behaviour can be obtained by modifying dopants.[27]

Fig. 3 illustrates that for the shortest annealing time (1 h), large grains are not frequently observed (only 0.8%), while for the longer annealing time (4 h), 90.6% of grains observed are large. The large grains have a size more than ten times that of the small grains (for 2 and 4 h annealed samples), which implies that the GB velocity for the large grains is larger than that for small grains.

3.2. Grain misorientation texture

From the grain size distribution analysis, all the small grains were consumed by the large grains after a 20 h anneal. The experimental observations of microstructural evolution suggest that some grains grow abnormally faster than other grains. Furthermore, this abnormal grain growth behaviour may also affect grain misorientations. As discussed in the introduction, the question is whether or not preferred Σ3 grain misorientations exist in polycrystalline $SrTiO_3$. Therefore, the measurement of textural evolution of grain misorientations through annealing is needed to resolve the Σ3 disagreement.

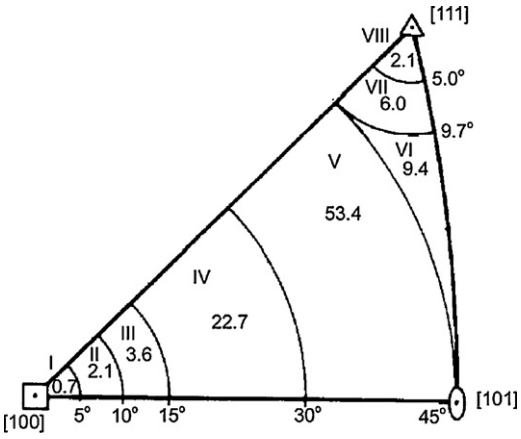

Fig. 4. Stereographic projection of the unit triangle showing the percentage of the Mackenzie random misorientation axis distribution falling in eight regions (after Mackenzie[32]). The regions (from I to VIII) are separated by solid curves at 5°, 10°, 15°, 30° and 45° from [1 0 0] and at 5° and 9.74° from [1 1 1].

The grain misorientation texture[28] is a function of three independent parameters (two for a misorientation axis and one for a misorientation angle). A common strategy for analyzing this 3-D data is to project it into one-dimensional space (misorientation angle)[29,30] or 2-D space (misorientation axis).[22,28,31] In this study, the grain misorientations are displayed in misorientation axis and angle space separately to obtain the misorientation axis and angle distributions for texture analysis.

First, to evaluate the distribution of the GB misorientation axes, the experimental data from different annealing times were compared with the theoretical Mackenzie random distribution[32]: the probability of a given random misorientation between two cubic crystals. The distribution of the misorientation axis can be displayed in a standard stereographic triangle for the random distribution,[32] as shown in Fig. 4. The triangle is divided into eight regions (I–VIII) showing the percentage of the random distribution in each region. The first five regions are divided by the curves at 5°, 10°, 15°, 30° and 45° away from [1 0 0]; the other three regions (data with axes orientated at angles greater than 45° from [1 0 0]) are divided by lines at 5° and 9.7° from [1 1 1]. Fig. 5 shows the GB misorientation distributions of 1 h (with 0.8% large grains) and 20 h (with 100.0% large grains) compared to the random distribution, for each of these eight regions. It is seen that the distribution for the 20 h sample is more like the random distribution than that of the 1 h sample.

In order to investigate why the GB axis distribution becomes more random for longer annealing times, the regions from the stereographic triangle with the largest deviations from random were analyzed further. In the 1 h sample, 82.4% of the total deviation from the random distribution occurs in four regions: I, IV, V and VIII. Three of these four regions include an area within 5° of a low-index axis: regions I, IV and VIII are near [1 0 0], [1 1 1] and [1 0 1], respectively. This suggests that GB misorientation axes near low-index directions dominate the deviation from randomness. Fig. 6 shows GB misorientation axis frequency near low-index directions as a function of annealing time in Nb-doped $SrTiO_3$ samples. It is clear that the fraction of the population near the three low-index directions reduces

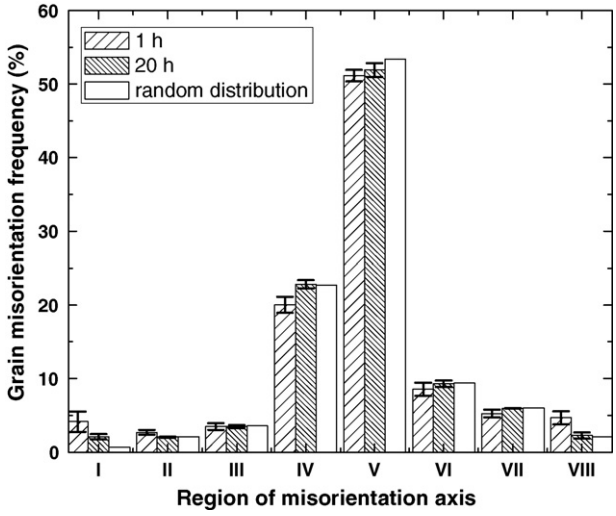

Fig. 5. Comparison of misorientation axis distribution in Nb-doped $SrTiO_3$ samples annealed for 1 and 20 h at 1425 °C in oxygen with the Mackenzie random distribution. Error bars indicate the standard deviation of grain misorientation frequency from different sets measured on three regions that contain at least 600 grains each.

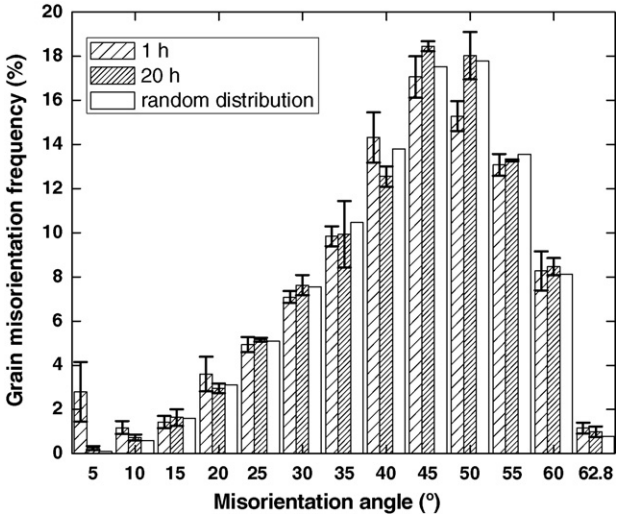

Fig. 7. Comparison of misorientation angle distribution in Nb-doped $SrTiO_3$ samples sintered for 1 and 20 h at 1425 °C in oxygen with the Mackenzie random distribution. Error bars indicate the standard deviation of grain misorientation frequency from different sets measured on three regions that contain at least 600 grains each.

with increasing annealing time. These data suggest that the distributions of small grains (99.2% in 1 h sample) and large grains (100.0% in 20 h sample) are different: the main difference is from the GB misorientation axes near low-index directions. Two effects are occurring during annealing (a) the large grain population is increasing in number and (b) grain growth is occurring. While it may be tempting to associate the 1 h data with the characteristics of the small grains and the 20 h data with those of the large grains, the effects of competitive grain growth cannot be ignored. However, as abnormal grain growth dominates the samples, the contribution to the GB misorientation axis distribution from near low-angle-axes segments reduces to approach the Mackenzie random distribution.

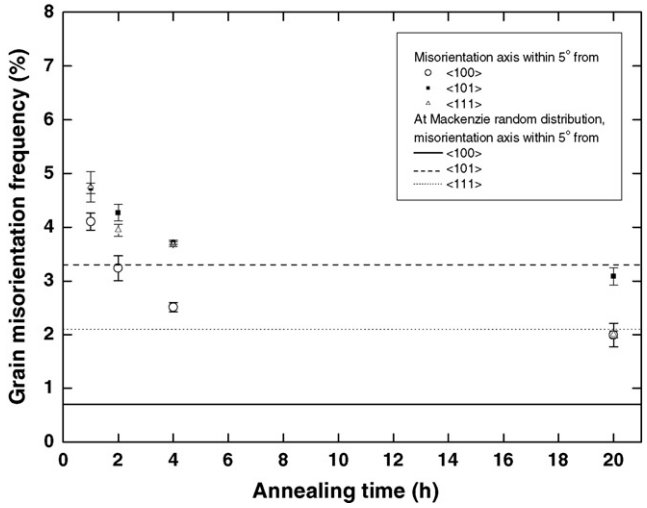

Fig. 6. Proportion of grain misorientations within 5° of low-index axes [1 0 0], [1 0 1] and [1 1 1] as a function of annealing time in Nb-doped $SrTiO_3$ samples sintered at 1425 °C in oxygen. Error bars indicate the standard deviation of grain misorientation frequency from different sets measured on three regions that contain at least 600 grains each.

After analyzing the GB misorientation axis distributions, the GB misorientation angle distributions were compared with the Mackenzie random distribution.[33] Fig. 7 shows the GB misorientation angle distribution in Nb-doped $SrTiO_3$ samples annealed for 1 h and 20 h together with the Mackenzie random distribution. There are two significant differences between the samples. Firstly, the large fraction of low-angle GBs present in the sample annealed for 1 h reduces in the sample annealed for 20 h. Secondly, the GB misorientation distribution for the 20 h annealed sample is more like the random distribution than is the 1 h sample, which is in agreement with the axis distribution analysis in the previous section. It should be noted that, for the 1 h annealed sample, the main deviation from the random distribution comes from small angle ($3° < \theta_m < 15°$) (35.9% of the total deviation) and large-angle ($40° < \theta_m < 50°$) (30.7% of the total deviation) misorientations.

Fig. 8 shows the frequency of GB misorientations of low-angle and large-angle GBs as a function of annealing time in Nb-doped $SrTiO_3$ samples. Populations of low-angle and large-angle GBs at the Mackenzie random distribution are illustrated using dotted and solid lines, respectively. The population of low-angle GB segments decreases and the population of large-angle GB segments increases with increasing annealing time to approach the Mackenzie random populations. The data support the idea that the GB misorientations of low- and large-angle GBs contribute to the reduction in deviation from randomness as abnormal grain growth progresses.

3.3. Σ3 misorientations

The evolution of grain misorientations can be explained by energy minimization during annealing as follows. During grain growth, energy minimization can be achieved in two ways. (i) The total grain boundary area is decreased. The higher veloc-

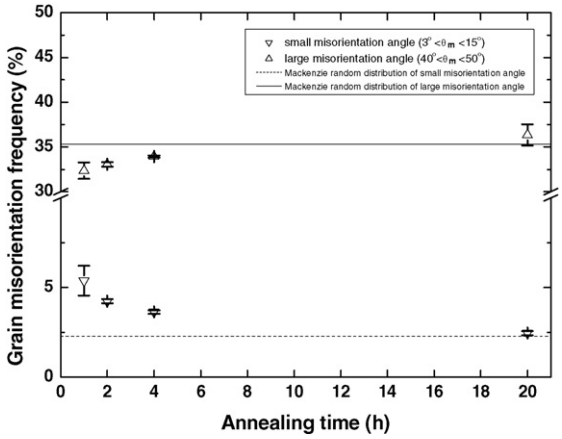

Fig. 8. Grain misorientations of low-angle ($3^\circ < \theta_m < 15^\circ$) and large-angle ($40^\circ < \theta_m < 50^\circ$) boundaries as a function of annealing time in Nb-doped $SrTiO_3$ samples sintered at 1425 °C in oxygen. Populations of low-angle and large-angle GBs at the Mackenzie random distribution are illustrated using dotted and solid lines, respectively. Error bars indicate the standard deviation of grain misorientation frequency from different sets measured on three regions that contain at least 600 grains each.

ity GBs (general, high-angle GBs[34]) will consume the lower velocity GBs. This results in a decrease in the population of low-angle and CSL GBs. (ii) The average grain boundary energy is decreased. The grain boundary character distribution will show an increase in the population of low-energy boundaries, i.e. low-angle and CSL GBs.[35,36] Seaton and Leach showed this second effect, where the density of Σ3 grain misorientations increased with annealing time between 0 and 60 min in donor-doped $BaTiO_3$.[16,17]

Fig. 9 shows the proportion of Σ3 GB misorientations from all grains and from small and large grains of Nb-doped $SrTiO_3$ samples as a function of annealing time. The Σ3 population

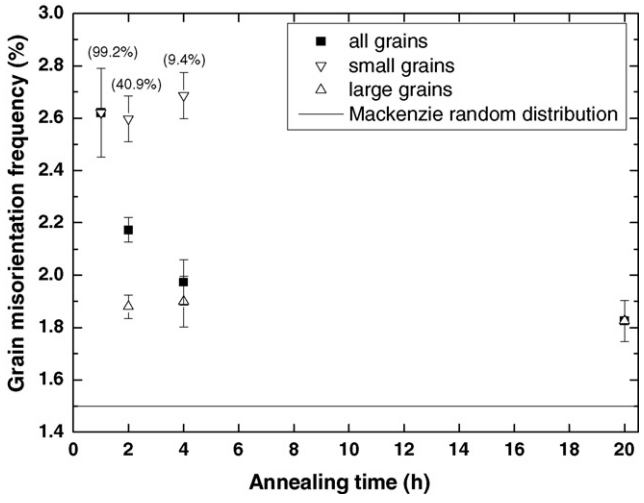

Fig. 9. Proportion of Σ3 misorientations from all grains and from small and large grains in Nb-doped $SrTiO_3$ samples as a function of annealing time. The percentage of small grains is given in brackets. Solid line indicates the population of the Σ3 GBs from the Mackenzie random distribution. Samples were sintered at 1425 °C in oxygen. Error bars indicate the standard deviation of grain misorientation frequency from different sets measured on three regions that contain at least 600 grains each.

decreases with increasing annealing time. According to Randle's analysis using the Mckenzie random distribution,[33,37] the Σ3 population for a random distribution of GBs is 1.5%. The result for the Σ3 population in the 20 h sample (~1.8%) is near Randle's figure, and similar values (~1.8–1.9%) of the Σ3 populations of the large grains were found in the 2 and 4 h samples. As both low-angle and Σ3 GB populations decrease with increasing annealing time, the results appear to be dominated by mechanism (i).

We assume that AGG effects on the sample can be removed by examining only the population of small grains. In Fig. 9, the population of Σ3 GBs in the small grains appears to be increasing with time (mechanism (ii)), although the error bars are large. Additionally, the grain size barely evolves (1.4–4.2 μm from 1 to 4 h annealing) compared with that of the large grains (5.4–28 μm for 1–4 h annealing). The fraction of small grains decreases significantly with annealing time, see Fig. 3. Small grains leave that population either by shrinking to zero volume or by joining the population of abnormal grains. This may explain the apparently stagnant grain growth, if the largest of the small grains are joining the abnormal grain population. Therefore, the grain growth in the sample as a whole appears to be dominated by mechanism (i).

In the case of undoped $SrTiO_3$, the sample annealed for 20 h has a lower proportion (1.1%) of large grains than the Nb-doped sample at 20 h (100%) (from Fig. 3). This suggests that the nucleation rate of the abnormal grains is lower in undoped samples than in Nb-doped samples. So, abnormal grains in the undoped sample have not consumed low-energy GBs from small grains to the same extent as in doped samples. Consequently for undoped $SrTiO_3$, mechanism (i) does not dominate (ii) to the same extent as for Nb-doped $SrTiO_3$, and Σ3 misorientations are found at a higher proportion (6.2%) than for doped samples. Thus, in $SrTiO_3$ the proportion of low-energy GBs (low-angle and CSL GBs) is strongly correlated with the grain growth behaviour, i.e. abnormal grain growth.

We now consider the apparently conflicting results in the literature. Ernst et al.[14] reported that Fe-doped $SrTiO_3$ had preferred Σ3 misorientations with five Σ3 GBs being found for 90 measurements based on Brandon's criterion. However, for undoped $SrTiO_3$, Saylor et al.[15] found 1276 Σ3 orientation segments in 75,088 GB segments (1.7%), and concluded that in their sample the proportion of Σ3 misorientations was near random. They suggested that the result of Ernst et al.[14] was due to TiO_2 excess and Fe-doping. We suggest that this discussion can be resolved by considering abnormal grain growth. From the measurement reported by Ernst et al.,[14] all 90 measured grains are small grains while Saylor's data come from both small (~30–120 μm) and large grains (~240–530 μm))[b]. In the population of small grains, the Σ3 misorientations increase in the population over time; however when abnormal grain growth dominates, the population of Σ3 misorientations decreases in the overall population with time.

[b] Grain size distributions are extracted from the Saylor's Fig. 1(b).

4. Conclusions

The frequency of low-energy GBs (i.e. low-angle and Σ3 GBs) observed in polycrystalline $SrTiO_3$ has been correlated to the annealing conditions. Nb doping increases the rate of grain growth and the nucleation rate of abnormal grains. Consequently the proportion of low-energy GBs is not only determined by annealing conditions but also by the mechanism of abnormal grain growth. The result in this study suggests that abnormal grain growth reduces the population of Σ3 GBs in $SrTiO_3$. An increase in the population of Σ3 GBs enhances the ion conductivity of $SrTiO_3$. Therefore, it is expected that for increased ion conductivity in $SrTiO_3$, a relatively high population of Σ3 GBs can be prepared by retarding abnormal grain growth.

Acknowledgements

The authors thank Prof. Hoffmann and Dr Bäurer for the provision of samples and helpful discussions. The authors would like to thank the European Commission for financial support under contract Nr. NMP3-CT-2005-013862 (INCEMS).

References

1. Minh, N. Q., Ceramic fuel-cells. *J. Am. Ceram. Soc.*, 1993, **76**, 563–588.
2. Takahash, T. and Iwahara, H., Ionic conduction in perovskite-type oxide solid solution and its application to solid electrolyte fuel cell. *Energy Convers.*, 1971, **11**, 105–111.
3. Chang, H. Y., Cheng, S. Y., Sheu, C. I. and Wang, Y. H., Core-shell structure of strontium titanate self-grown by a hydrothermal process for use in grain boundary barrier layers. *Nanotechnology*, 2003, **14**, 603–608.
4. Shen, H., Song, Y. W., Gu, H., Wang, P. C. and Xi, Y. M., A high-permittivity $SrTiO_3$-based grain boundary barrier layer capacitor material single-fired under low temperature. *Mater. Lett.*, 2002, **56**, 802–805.
5. Rodrigues, R. P., Chang, H. J., Ellis, D. E. and Dravid, V. P., Electronic structure of pristine and solute-incorporated $SrTiO_3$. II. Grain-boundary geometry and acceptor doping. *J. Am. Ceram. Soc.*, 1999, **82**, 2385–2394.
6. Chiang, Y. M., Birnie III, D. P. and Kingery, W. D., *Physical Ceramics—Principles for Ceramic Science and Engineering*. John Wiley & Son, Inc., New York, 1997.
7. Kronberg, M. L. and Wilson, F. H., Secondary recrystallization in copper. *T. Am. I. Min. Met. Eng.*, 1949, **185**, 501–514.
8. Brandon, D. G., Structure of high-angle grain boundaries. *Acta Metall.*, 1966, **14**, 1479–1484.
9. Ogawa, H., Demura, M., Yamamoto, T. and Sakuma, T., Estimation of PTCR effect in single grain boundary of Nb-doped $BaTiO_3$. *J. Mater. Sci. Lett.*, 1996, **15**, 537–538.
10. Hayashi, K., Yamamoto, T. and Sakuma, T., Grain orientation dependence of the PTCR effect in niobium-doped barium titanate. *J. Am. Ceram. Soc.*, 1996, **79**, 1669–1672.
11. Kienzle, O., Exner, M. and Ernst, F., Atomistic structure of Sigma = 3, (1 1 1) grain boundaries in strontium titanate. *Phys. Status Solidi A: Appl. Res.*, 1998, **166**, 57–71.
12. Ernst, F., Kienzle, O. and Rühle, M., Structure and composition of grain boundaries in ceramics. *J. Eur. Ceram. Soc.*, 1999, **19**, 665–673.
13. Hutt, S., Kostlmeier, S. and Elsasser, C., Density functional study of the Sigma 3 (1 1 1) 1(1)over-$\bar{0}$ symmetrical tilt grain boundary in $SrTiO_3$. *J. Phys.Condens. Matter*, 2001, **13**, 3949–3960.
14. Ernst, F., Mulvihill, M. L., Kienzle, O. and Rühle, M., Preferred grain orientation relationships in sintered perovskite ceramics. *J. Am. Ceram. Soc.*, 2001, **84**, 1885–1890.
15. Saylor, D. M., El Dasher, B., Sano, T. and Rohrer, G. S., Distribution of grain boundaries in $SrTiO_3$ as a function of five macroscopic parameters. *J. Am. Ceram. Soc.*, 2004, **87**, 670–676.
16. Seaton, J. and Leach, C., Evolution of low sigma grain boundaries in PTC thermistors during sintering. *J. Eur. Ceram. Soc.*, 2005, **25**, 3055–3058.
17. Seaton, J. and Leach, C., Formation and retention of low Sigma interfaces in PTC thermistors. *Acta Mater.*, 2005, **53**, 2751–2758.
18. Park, M. B., Shih, S. J. and Cockayne, D. J. H., The preferred CSL misorientation distribution in polycrystalline $SrTiO_3$. *J. Microsc. Oxford*, 2007, **227**, 292–297.
19. Bäurer, M., Kungl, H. and Hoffmann, M. J., Influence of Sr/Ti stoichiometry on the densification behaviour of strontium titanate. *J. Am. Ceram. Soc.*, 2009, **92**, 601–606.
20. Shih, S. J., Park, M. B. and Cockayne, D. J. H., The interpretation of indexing of high Sigma CSL grain boundaries from ceramics. *J. Microsc. Oxford*, 2007, **227**, 309–314.
21. Humphreys, F. J., Review—grain and subgrain characterisation by electron backscatter diffraction. *J. Mater. Sci.*, 2001, **36**, 3833–3854.
22. Lee, J. S., Misorientation distribution of a Mn–Zn ferrite sample with abnormal grain growth. *J. Ceram. Process Res.*, 2004, **5**, 179–186.
23. Underwood, E. E., *Quantitative Stereology*. Addison-Wesley, Reading, 1970.
24. Peng, C. J. and Chiang, Y. M., Grain-growth in donor-doped $SrTiO_3$. *J. Mater. Res.*, 1990, **5**, 1237–1245.
25. Bae, C., Park, J. G., Kim, Y. H. and Jeon, H., Abnormal grain growth of niobium-doped strontium titanate ceramics. *J. Am. Ceram. Soc.*, 1998, **81**, 3005–3009.
26. Chung, S. Y. and Kang, S. J. L., Intergranular amorphous films and dislocations-promoted grain growth in $SrTiO_3$. *Acta Mater.*, 2003, **51**, 2345–2354.
27. Chung, S. Y., Yoon, D. Y. and Kang, S. J. L., Effects of donor concentration and oxygen partial pressure on interface morphology and grain growth behavior in $SrTiO_3$. *Acta Mater.*, 2002, **50**, 3361–3371.
28. Randle, V. and Ralph, B., The coincident axial direction (CAD) approach to grain-boundary structure. *J. Mater. Sci.*, 1988, **23**, 934–940.
29. Bystrzycki, J. and Varin, R. A., Microstructure and microtexture in powder-extruded monolithic NiAl and NiAl-HfC alloy. *Intermetallics*, 1998, **6**, 277–289.
30. Randle, V., Interfacial geometry in simulated rolling and recrystallization textures. *Model. Simul. Mater. Sci.*, 1996, **4**, 455–472.
31. Lee, J. S., Kim, D. Y., Fleig, J. and Joachim, M., Geometry and electrical properties of grain boundaries in manganese zinc ferrite ceramics. *J. Am. Ceram. Soc.*, 2004, **87**, 1895–1902.
32. Mackenzie, J. K., Distribution of rotation axes in random aggregate of cubic crystals. *Acta Metall.*, 1964, **12**, 223–225.
33. Mackenzie, J. K., 2nd paper on statistics associated with the random disorientation of cubes. *Biometrika*, 1958, **45**, 229–240.
34. Sutton, A. P. and Balluffi, R. W., *Interfaces in Crystalline Materials*. Oxford University Press, Oxford, 1995, pp. 526–573.
35. Dimou, G. and Aust, K. T., Relative energies of grain-boundaries near a coincidence orientation relationship in high-purity lead. *Acta Metall.*, 1974, **22**, 27–32.
36. Randle, V., Application of electron backscatter diffraction to grain boundary characterisation. *Int. Mater. Rev.*, 2004, **49**, 1–11.
37. Randle, V., Relationship between coincidence site lattice, boundary plane indices, and boundary energy in nickel. *Mater. Sci. Technol.*, 1999, **15**, 246–252.